

MODULATED CRYSTAL STRUCTURES OF GREENALITE AND CARYOPILITE: A SYSTEM WITH LONG-RANGE, IN-PLANE STRUCTURAL DISORDER IN THE TETRAHEDRA SHEET

STEPHEN GUGGENHEIM¹

*Department of Earth and Environmental Sciences, University of Illinois at Chicago, 845 W. Taylor Street,
Chicago, Illinois 60680, U.S.A.*

RICHARD A. EGGLETON¹

Department of Geology, Australian National University, Canberra, ACT 0200, Australia

ABSTRACT

High-resolution transmission electron microscope (TEM) images confirm that greenalite and caryopilite are modulated 1:1 phyllosilicates. The octahedrally coordinated Fe (greenalite) and Mn (caryopilite) form trioctahedral sheets. Six-member rings of tetrahedra link to form triangular islands four or five tetrahedra across, with each island coordinating to one octahedral sheet. Adjacent islands are inverted and link to the neighboring octahedral sheet, which results in a triply-intersecting corrugation for the tetrahedral sheet. Islands vary in numbers of tetrahedra about a mean dictated by the octahedral sheet dimension. Island separations range about a mean distance within the X - Y plane, with island alignment fluctuating as a function of lattice vectors defined by the octahedral sheet. The tetrahedra thus show limited short-range order (spanning to five octahedra), but long-range disorder. Linkages of tetrahedra between islands are apparently completely disordered. Because of this disorder, there is no definable unit-cell. Fourier calculations involving non-repeating structures cannot use unit-cell fractional coordinates and Miller indices. We calculated diffraction patterns by finding the real-space coordinates of every atom in the model relative to a defined origin. The reciprocal space variable, d^* , is sampled at intervals of 0.005 Å to build the continuous Fourier transform of the model. Discrete polytypes of $1T$ and $1M$ for greenalite and caryopilite, respectively, were identified. Where grains contain mixtures, the relative abundance of each polytype is related to composition, with the dominant polytype based on minimizing misfit between the sheets of octahedra and of tetrahedra. Stacking in greenalite and caryopilite is defined by the relative positions of adjacent octahedral sheets and, therefore, limits on the displacements of neighboring domains of silicate rings within (001) are possible. Domain boundary linkages, however, cannot be determined precisely by using either diffraction or imaging data.

Keywords: greenalite, caryopilite, serpentines, modulated structures, superstructure, phyllosilicates, polytypism, Fourier synthesis of disordered structures, electron diffraction.

SOMMAIRE

Les images obtenues par microscopie électronique en transmission à haute résolution confirment l'hypothèse voulant que la greenalite et la caryopilite sont des phyllosilicates 1:1 modulés. Les octaèdres contenant le Fe (greenalite) et le Mn (caryopilite) forment des feuilletts trioctaédriques. Des anneaux de six tétraèdres forment des agencements en flots triangulaires quatre ou cinq tétraèdres de large, chacun des flots étant coordonné à un feuillet d'octaèdres. Des flots adjacents sont inversés et rattachés au feuillet d'octaèdres avoisinant, avec comme résultat une modulation des feuilletts de tétraèdres en trois directions. Ces flots contiennent un nombre variable de tétraèdres, mais le nombre moyen dépend de la dimension du feuillet d'octaèdres. Leur séparation moyenne dans le plan X - Y a aussi une variance associée, l'alignement des flots étant géré par la fluctuation des vecteurs réticulaires définis par le feuillet d'octaèdres. Les tétraèdres montrent ainsi un certain degré d'ordre (limité à une séquence de cinq octaèdres), mais sont désordonnés sur une plus grande échelle. Les agencements de tétraèdres entre flots seraient complètement désordonnés. Vu ce désordre, il est impossible de définir une maille élémentaire. Des calculs faisant appel à la transformation de Fourier de structures non répétées ne pourraient utiliser l'indiciage de Miller et les coordonnées fractionnelles des atomes dans une maille. Nous avons calculé des spectres de diffraction X en spécifiant les coordonnées des atomes dans l'espace en termes absolus par rapport à une origine fixe. La variable dans l'espace réciproque, d^* , est évaluée à un intervalle de 0.005 Å afin de construire une synthèse de Fourier continue du modèle. Nous reconnaissons dans ce modèle les polytypes $1T$ et $1M$ de la greenalite et de la caryopilite, respectivement. Où les grains contiennent des mélanges, la proportion de chacun des polytypes dépend de la composition, le polytype dominant étant celui qui réussit le mieux à minimiser

¹ E-mail addresses: xtal@uic.edu, rae653@anugpo.anu.edu.au

le décalage entre les feuillets d'octaèdres et de tétraèdres. La séquence d'empilements dans la greenalite et la caryopilite dépend alors des positions relatives des feuillets d'octaèdres adjacents et, donc, des limites dans les déplacements possibles de domaines adjacents d'anneaux dans le plan (001). En revanche, il est impossible de préciser les agencements dans les zones inter-domaines en utilisant les données de diffraction ou les images obtenues.

(Traduit par la Rédaction)

Mots-clés: greenalite, caryopilite, serpentines, structures modulées, surstructure, phyllosilicates, polytypisme, synthèse de Fourier des structures désordonnées, diffraction d'électrons.

INTRODUCTION

In phyllosilicates, octahedrally coordinated cations generally coordinate to either oxygen atoms or OH groups; the oxygen atoms belong also to the silicate tetrahedra. Thus, the apical oxygen atoms form a junction between a continuous octahedral sheet (= sheet of octahedra) and a tetrahedral sheet (= sheet of tetrahedra). The oxygen atoms have a lateral spacing congruent with both the octahedra and the tetrahedra. In kaolinite and the chrysotile variety of serpentine, for example, where there are relatively small octahedrally coordinated cations such as Mg and Al, the tetrahedral sheet is continuous because the Si-to-Si spacings match the spacings from apical oxygen to apical oxygen defined by the octahedra. Large cations such as Fe²⁺ and Mn²⁺, however, prevent such a fit. In these structures, the anion-to-anion spacing of the common junction cannot match the Si-to-Si spacings of the tetrahedra; thus, an inversion of tetrahedra or some other structural perturbation or modulation is necessary to reset the spacing after a short run of tetrahedra. It is this misfit between the octahedral sheet and the tetrahedral sheet that appears to be the underlying principle in the formation of modulated phyllosilicates (Guggenheim & Eggleton 1987, 1988).

Greenalite is the Al-poor and Fe²⁺-rich serpentine, and caryopilite is the Mn analogue. They form in low-energy environments, commonly in either very low-grade metamorphic rocks or in hydrothermal veins or replacements. The minerals are almost always fine-grained, and usually intermixed with quartz and either Fe or Mn silicates or oxides, respectively. Greenalite and caryopilite form a (homologous) series of closely related modulated structures (Guggenheim *et al.* 1982). Electron-diffraction patterns (Guggenheim *et al.* 1982) derived from single crystals of both minerals show that a noncommensurate superlattice exists, which produces satellite reflections around $k = 3n$ reflections in the $hk0$ plane (Fig. 1). Spacings measured between the subcell and the superlattice reflections (Guggenheim *et al.* 1982) indicate that approximately 23-Å domains within (001) exist in greenalite, and approximately 17-Å domains exist in caryopilite. An Al-poor, Mg-Zn-Mn-Fe-bearing phase has approximately 30-Å domains (Guggenheim & Bailey 1989).

Samples analyzed using micro-analytical techniques from pure areas always show an excess of Si and a deficiency in octahedrally coordinated cations, on the basis of an ideal structure and composition of serpentine, with a total cation charge of +14. A change in configuration of the ring of tetrahedra, from 6-fold rings within the domains to other configurations at domain boundaries, would explain the excess in Si and deficiency in octahedrally coordinated cations (Guggenheim *et al.* 1982). The spacings of approximately 17 Å, 23 Å, and 30 Å are related to domains of rings of tetrahedra attached to a continuous octahedral sheet, with the smaller domain required for the sheet with the larger average octahedrally coordinated cation. The spacings appear to be step-like and not continuous (Guggenheim & Bailey 1989), thereby suggesting that in caryopilite, the domains have a diameter of three rings of tetrahedra whereas in greenalite, the number is four. Although Guggenheim *et al.* (1982) presented an idealized model for the structure of greenalite, they were unable to obtain high-resolution electron-optical images to substantiate the model. They did, however, produce a laser-optical diffraction pattern of $hk0$ reflections that simulates the observed pattern closely.

Serpentine-group minerals can also have adjacent layers displaced to form different polytypic arrangements. Although there are twelve ideal polytypes in the serpentines, these may be divided into four groups of three polytypes each, depending on the occupancy of certain interstices among the octahedra (Bailey 1969). Where stacking disorder is severe, as in greenalite and caryopilite, group-A structures and group-C structures may be thought of as $1M$ and $1T$ polytypes, respectively, because random stacking makes the polytypes within each group indistinguishable. Guggenheim *et al.* (1982) determined that two polytypes ($1M$ and $1T$) are present in all samples of greenalite and caryopilite studied, with greenalite predominantly composed of the $1T$ polytype, and caryopilite mostly consisting of the $1M$ polytype. Single-crystal X-ray patterns from an imperfect crystal of greenalite indicate that the two intergrown polytypes are fixed in relative orientations. Guggenheim *et al.* were unable to determine if the intergrown polytypes are related to the structural modulation, nor could they definitively argue that the polytypes are a result of differences in the size of Fe and Mn.

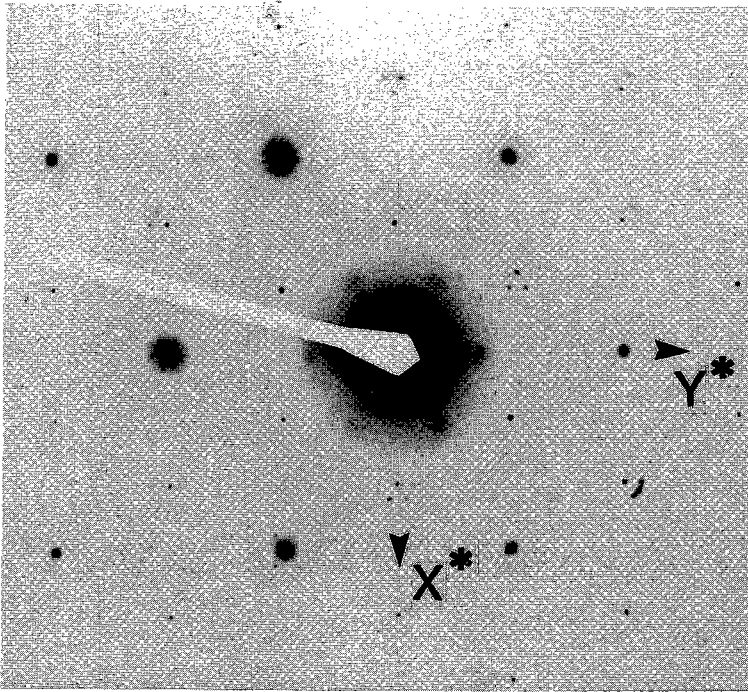


FIG. 1. Electron-diffraction pattern showing the $hk0$ net of greenalite, Cartagena mining district, La Union, Murcia, Spain.

Our purpose in the present paper is to re-examine the earlier model in view of additional data, primarily better electron-diffraction patterns and electron-optical images. We illustrate several approaches to the interpretation and calculation of diffraction data from crystals that are imperfect.

EXPERIMENTAL

Since our previous study (Guggenheim *et al.* 1982), several samples from new localities have become available (Table 1). Table 2 provides electron-microprobe data for pure greenalite, obtained using a Cameca Microbeam electron microprobe. Because of the fine-grained nature of the material, an energy-dispersion system (EDS) was used at 15 kV and 4.8 nA, with a focused beam. We used MgO, CaAl₂O₄, CaSiO₃, Fe, and MnO as primary synthetic standards. The data were processed with the SILICP program and ZAF corrections (Ware 1991). Samples are within the range of composition given by Guggenheim *et al.* (1982). Although the sample from the Overlook gold deposit has relatively small Al and Mn contents, and a high Fe content (Rasmussen *et al.* 1998), it compares closely in composition to the Gunflint samples of greenalite described by Guggenheim *et al.* (1982).

TABLE 1. SAMPLES OF CARYOPILITE AND GREENALITE STUDIED

1.	Caryopilite, Molinello mine, near Chiavari, Liguria, Italy. Thin vein of hydrothermal origin; intimately intermixed with parsettensite and an undescribed mineral. Sample #C1979a.
2.	Caryopilite, Långban, Sweden. Veins of hydrothermal origin; sparsely distributed submicroscopic grains in nearly pure gonyerite. Harvard #112842; see Frondel (1955).
3.	Greenalite, San Valentin Cartagena mining district, La Union, Murcia, Spain. Subvolcanic, hydrothermal, late Tertiary replacement of limestone; see Guggenheim <i>et al.</i> (1982).
4.	Greenalite, West Peko deposit, Tennant Creek, Northern Territories, Australia. Hydrothermal mineralization in Proterozoic epigenetic ironstone; associated with chalcopyrite, galena, gold, magnetite, quartz, minnesotaite, Fe-bearing talc, stilpnomelane, and bismuth minerals. Sample #WP13-624.
5.	Greenalite, Overlook gold deposit, northeastern Washington, U.S.A. Epigenetic replacement suite or a greenschist-grade metamorphism overprinted by Tertiary hydrothermal mineralization; associated with fayalite, talc, pyrrhotite, chalcopyrite, magnetite, gold, mimesotäite, calcite, and quartz. Sample #OLC30-720.

A JEOL 100CX microscope was used for rapid examination of grain mounts to produce diffraction patterns along [001]*; JEOL 200CX and JEOL 4000FX microscopes were used to examine ion-thinned samples for high-resolution imaging. Grain mounts were prepared by crushing material, mixing with alcohol,

TABLE 2. RESULTS OF ELECTRON-MICROPROBE ANALYSES OF GREENALITE

	West Peko	Overlook	Cartagena*
SiO ₂ wt.%	35.57	35.82	35.9
Al ₂ O ₃	0.31	0.05	0.16
FeO **	46.80	50.23	47.8
MnO	3.53	0.03	1.78
MgO	3.26	2.37	4.13
Total	89.47	88.50	89.77
Proportion of atoms based on 7 atoms of oxygen			
Si	2.10	2.14	2.10
Al	0.02	0.00	0.01
Fe	2.31	2.51	2.34
Mn	0.18	0.00	0.09
Mg	0.29	0.21	0.36
Proportion of atoms based on 3 (Fe + Mn + Mg)			
Si	2.27	2.36	2.26
Al	0.02	0.00	0.01
Fe	2.50	2.77	2.52
Mn	0.19	0.00	0.09
Mg	0.31	0.23	0.39
Σoxygen (tet)	3.00	3.00	3.00

* from Guggenheim *et al.* (1982). ** All Fe assumed FeO.

and placing a drop of the mix onto a holey carbon grid. Ion-thinned specimens were prepared following standard procedures (*e.g.*, Guggenheim *et al.* 1982).

An important feature of all greenalite and caryopilite $hk0$ nets (Fig. 1) is that the superlattice reflections form hexagons of satellites (Guggenheim *et al.* 1982) directed along the three pseudohexagonal b^* axes (*i.e.*, $[010]^*$, $[110]^*$, and $[1\bar{1}0]^*$). Overexposed nets may show second-order superlattice reflections and, in one grain of caryopilite from Långban, a third-order superlattice reflection was observed.

In contrast with the earlier study, individual grains were found that produced characteristic $h0l$ and $0kl$ diffraction patterns (Figs. 2, 3). The $h0l$ pattern for greenalite is based on an orthohexagonal cell ($\beta = 90^\circ$), whereas caryopilite has a monoclinic cell ($\beta = 104.6^\circ$), in accord with the dominant $1T$ (group-C) and $1M$ (group-A) polytypes for greenalite and caryopilite, respectively. In theory, the $h0l$ patterns should not show those superlattice reflections around $k = 3n$ subcell reflections because the $[100]^*$ direction bisects the superlattice nodes (Fig. 1). In practice, however, primarily owing to the small spacing between superlattice nodes and possibly also to the curvature of Ewald's sphere, deformation of the specimen, and strain features, both adjacent superlattice reflections appear on the net.

High-resolution electron-optical bright-field images were produced by allowing all reflections in either the $h0l$ or the $0kl$ nets to pass through an aperture with a diameter of 3.0 \AA^{-1} . The image projected (Fig. 4) down $[100]$ shows dark undulating bands separated by lighter

areas with electron density organized into dots or short regions of poorly resolved dots. Although not necessarily in Figure 4, on the average, there are nearly equal numbers of dots that associate with either one or the other of the adjacent dark bands. Regions of low electron-density are readily apparent. Occasionally, a "pillar" is formed connecting the adjacent dark lines where two dots line up along $[001]$. The important features are (1) the general lack of positional regularity of these dots along $[010]$, and (2) the nearly equal number of dots associated with each dark band.

The image (Fig. 5) of the structure along $[010]$ shows rows of black spots repeating at approximately 3-\AA intervals. Dots are present in the region between these rows, but these dots are very poorly resolved, and it is difficult to locate regions of low electron-density. Such regions become more obvious if the figure is viewed looking parallel to the rows of spots at an acute angle to the page. The important feature of this image is that there is no regularity to the positions of dots along $[100]$.

RESULTS AND DISCUSSION

The dark undulating bands in the image (Fig. 4) formed from the projection down $[100]$ are intuitively interpreted as a continuous octahedral sheet separated by dots that represent tetrahedra. There are nearly equal numbers of tetrahedra that associate with either one or the other of the adjacent octahedral sheets on average. The dominant theme is a general lack of positional regularity along $[010]$. Figure 4 shows several examples of order-disorder. The octahedrally coordinated cations are ordered parallel to $[010]$. The tetrahedra may show three or four repeated alternations of islands pointed "up" and islands pointed "down" of the same size before there is a change, thus revealing some short-range order but a lack of long-range order parallel to $[010]$. The y -position of an island of tetrahedra may be the same as that for those islands above and below over 6–10 layers (commonly) or a few tens of layers (less commonly), revealing long-range order parallel to $[001]^*$.

We infer that the image (Fig. 5) of the projection of the structure down $[010]$ shows iron atoms resolved as rows of black spots along $[100]$. Very poorly resolved dots relating to tetrahedra are present in the region between the octahedral sheets. In some cases, these "dots" become smeared out completely; further interpretation of this net is problematic because superlattice reflections from two directions were unavoidably admitted into the aperture (see comments above).

Extreme positional disorder is commonly associated with streaking or diffuseness in diffraction patterns. For example, random displacements of 1:1 layers along $[001]$ by $+b/3$ or along the pseudohexagonal b axes in the lizardite variety of serpentine produces streaking in the $0kl$ net parallel to $[001]^*$ for $k \neq 3n$ reflections. Although a similar diffraction effect is observed for

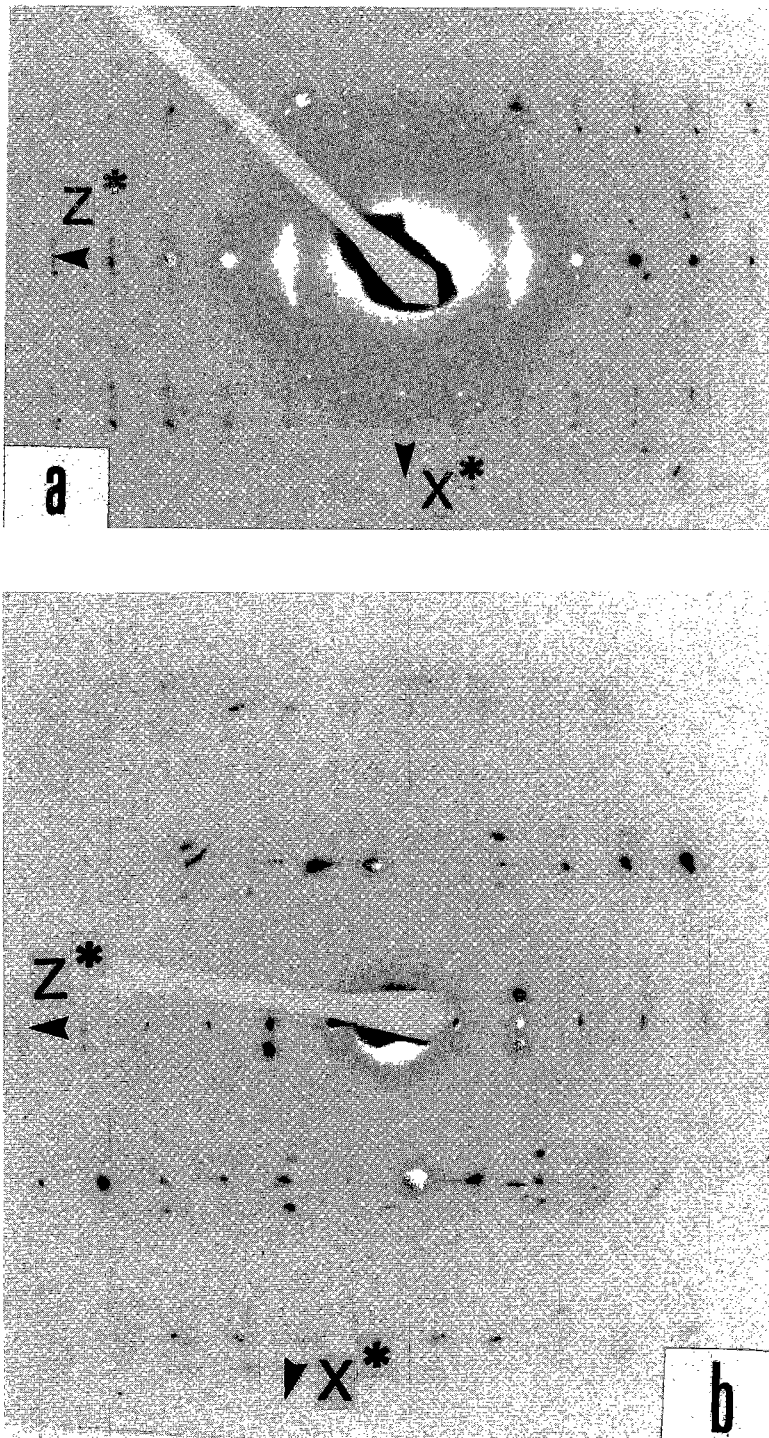


FIG. 2. Electron-diffraction pattern showing the $h0l$ net in (a) greenalite-1T, La Union, Murcia, Spain, and (b) caryopilite-1M, Liguria, Italy.

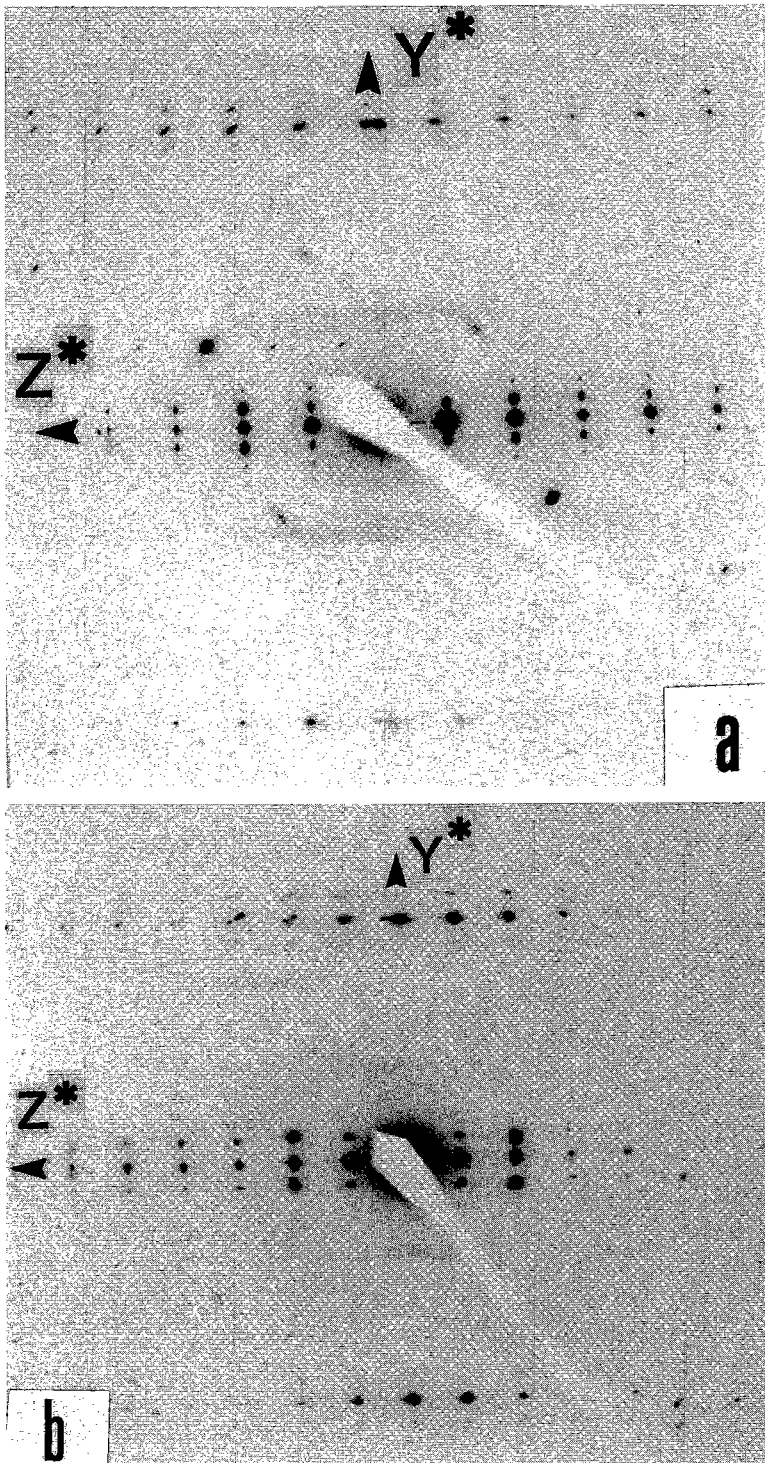


FIG. 3. Comparison of the Ok_l nets in (a) greenalite, La Union, Murcia, Spain, and (b) caryopilite, Liguria, Italy. The superlattice spacings are slightly different for the two nets. The subcell reflections form $00l$ and $06l$ rows.

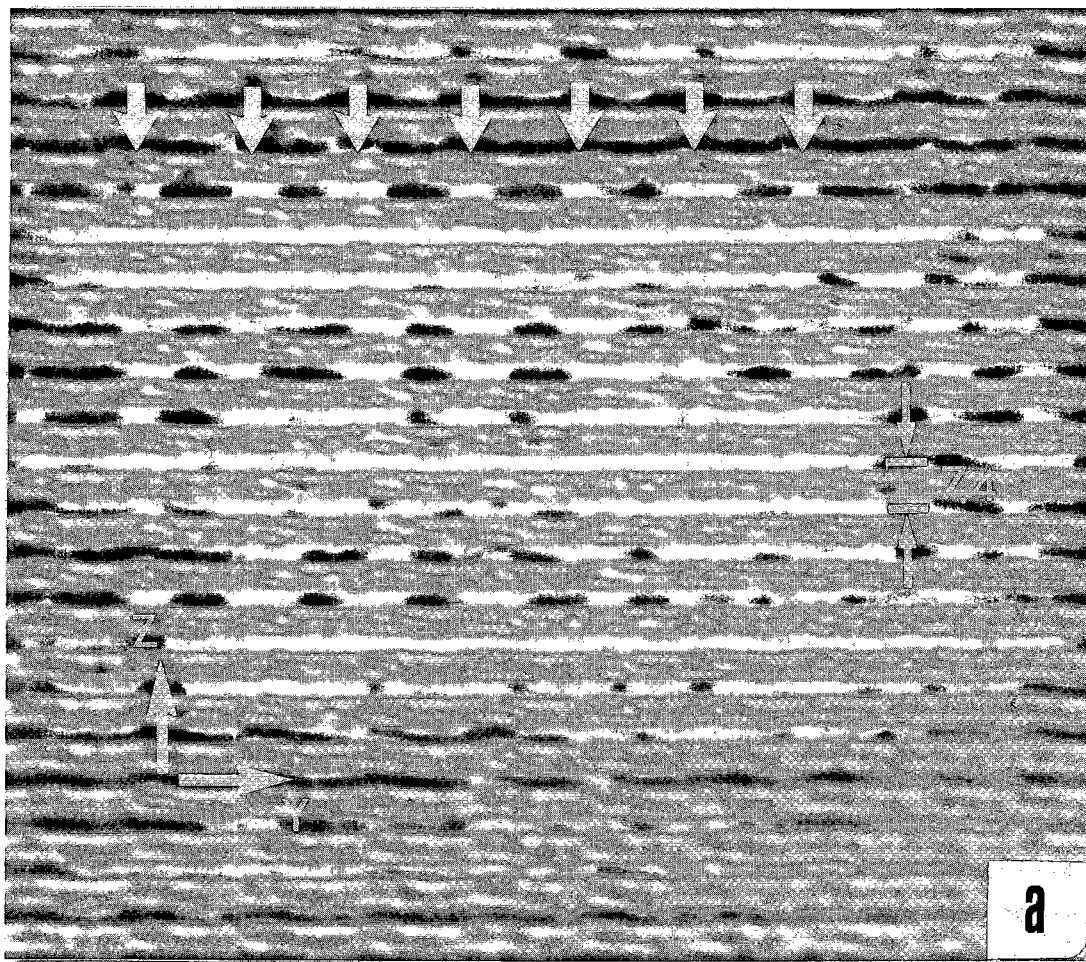


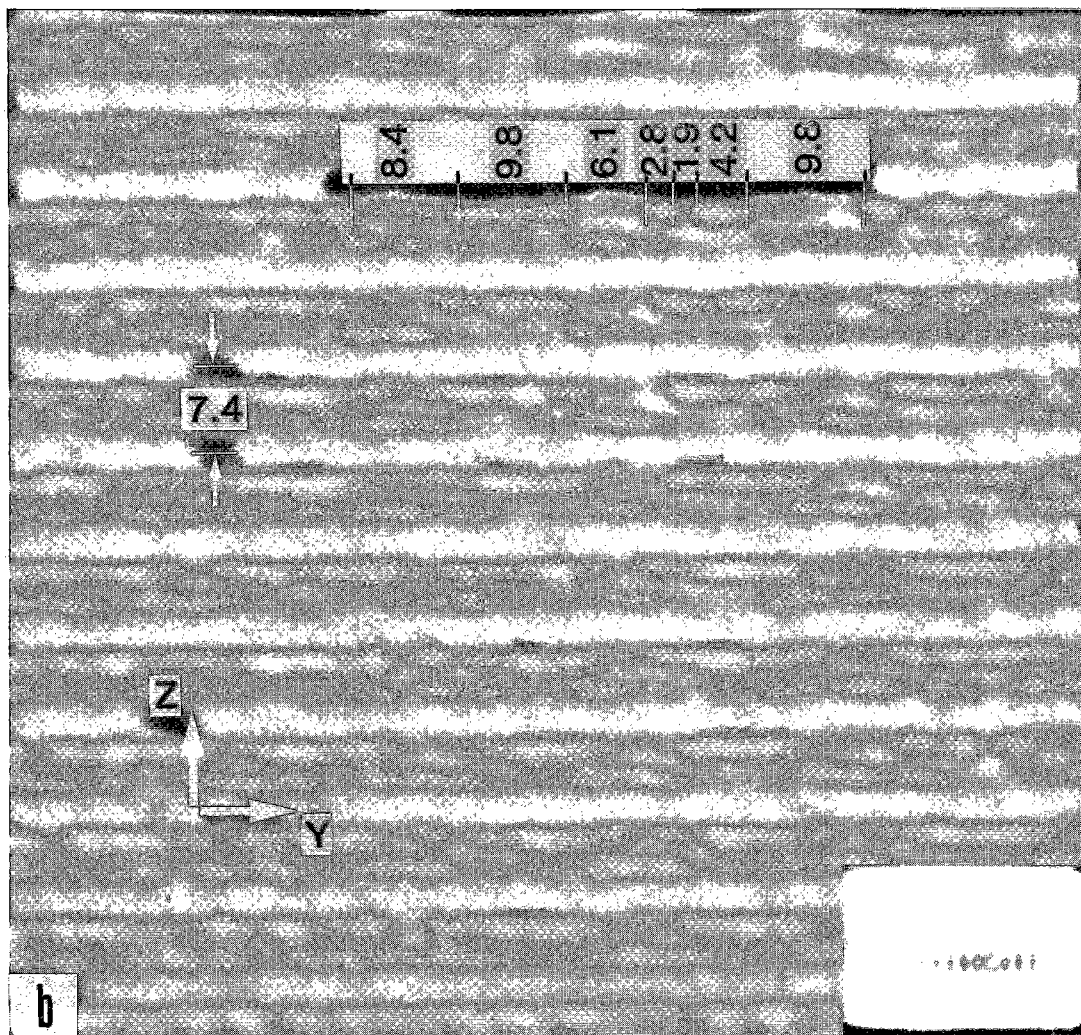
FIG. 4. HRTEM images projected down [100] for caryopilite, Långban, Sweden, as obtained with a JEOL 200CX instrument. The image in (a) is at low magnification to illustrate "columns" parallel to [001], as noted by arrows in the upper part of the figure. The columns may extend for thousands of layers along [001], although they rarely line up for more than a few tens of layers (note the loss of regularity on the right side of the figure). The high-magnification image (b) shows the spacings of "dots", which are interpreted as silicate tetrahedra. All dimensions are given in Ångströms. The cell origin is arbitrary.

the subcell reflections for greenalite and caryopilite, streaking or diffuseness is not observed for the superlattice reflections around $k = 3n$ subcell reflections. Instead, sharp superlattice nodes occur in the $hk0$, $0kl$, and $h0l$ nets, although the images indicate extreme positional disorder among the tetrahedra.

Guinier (1963, p. 297-304) considered the diffraction effects from a one-dimensional imperfect crystal, where the distance between two successive lattice points varies about an average value (a) and the distance between any pair is not related to the distance between adjacent pairs. In a perfect lattice, the distribution of inter-lattice-point distances is a series of line maxima at

exactly a , $2a$, $3a$, $4a$, etc., with no other inter-lattice spacings. In the imperfect crystal considered by Guinier, the distribution of inter-lattice-point spacings shows a sharp, high maximum centered at a spacing equal to a , a broader, lower peak around $2a$, and by $4a$ the inter-lattice-point distribution has become very poorly defined. The Fourier transform of such a system produces a series of maxima, with a rapid decrease in intensity and an increase in diffuseness from the first maximum to the second, and a general loss of discrete maxima beyond.

In greenalite and caryopilite, electron-diffraction patterns of the $hk0$ net show satellite reflections



around the $k = 3n$ reflections that form hexagons, with corners directed along the three pseudo-hexagonal b^* axes. If just the superlattice is considered, then the one-dimensional system is analogous to the greenalite – caryopilite structure by defining the lattice points at domain centers and by considering distances between domain centers within (001). Thus, each pseudo-hexagonal b^* axis may be considered a linear lattice in reciprocal space. A pattern results with a maximum intensity (node) on the superlattice at $n = 1$ and very rarely at $n = 2$. We infer that distances between domain centers fluctuate irregularly about an average value in a similar way along each of these directions. The relative sharpness of these superlattice nodes indicates that the widths of the domains vary within small limits, as has been previously suggested by Guggenheim *et al.*

(1982) on the basis of arguments relating to the misfit between sheets of tetrahedra and of octahedra.

The electron diffraction and TEM image results show that there is no well-defined periodicity in the XY plane, but that the tetrahedral sheet does have a structural element repeating with a pseudo-orthohexagonal supercell, ranging in dimensions ($a \times b$) from about $26.5 \times 46 \text{ \AA}$ for greenalite to $19.6 \times 34 \text{ \AA}$ for caryopilite.

Guggenheim *et al.* (1982) recognized that random displacements of domains parallel to (001) are an essential part of the greenalite and caryopilite structures, and introduced displacement vectors to generate the optical diffraction pattern given in their Figure 9. In effect, these vectors produce random displacements that eliminate the unit cell of their

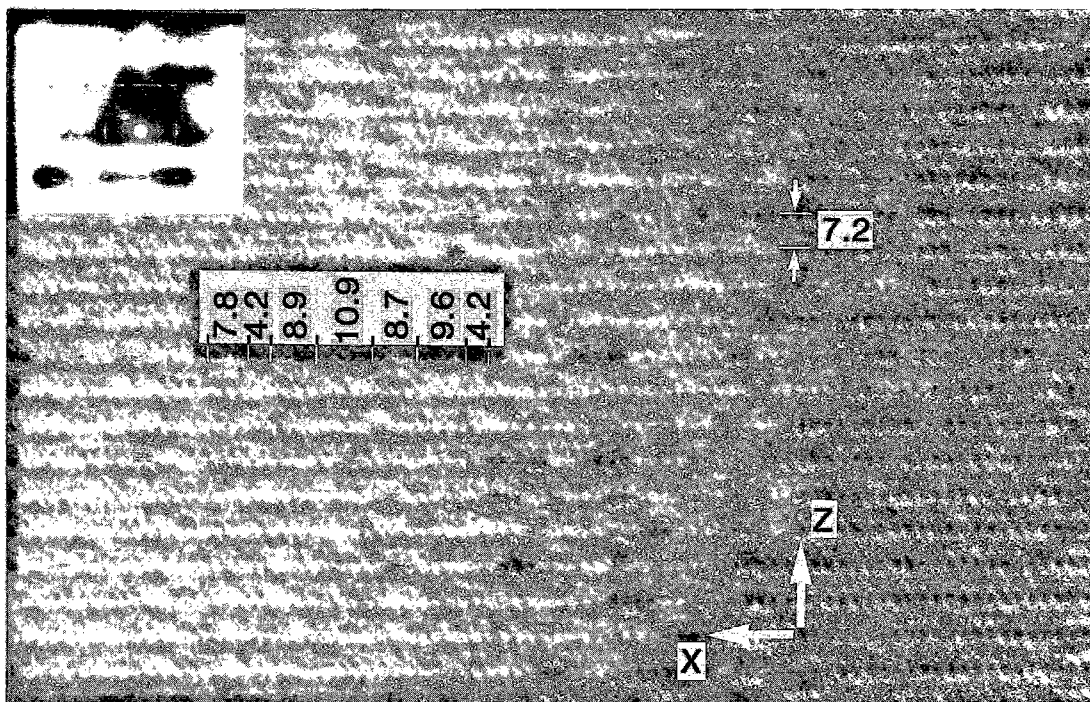


FIG. 5. High-resolution electron-optical image down [010] for greenalite-1*T*, La Union, Murcia, Spain, as obtained with a JEOL 400FX instrument. Note the well-resolved black spots forming rows, which are interpreted as resolved Fe atoms. The series of dimensions (in Å) refer to the alternating light and dark regions in the tetrahedral sheet.

idealized model. However, constraints could not be placed on the sizes of the vectors beyond the suggestion that they are related to "anion-to-anion distances". Figure 9 of Guggenheim *et al.* (1982) closely resembles the $hk0$ diffraction pattern of greenalite, and the results of their diffraction experiments remain valid for the conceptual model presented below. However, it now becomes possible to deduce the nature of the displacement vectors from a conceptual model and to use this information to simulate the two-dimensional diffraction involving the superlattice in the OkI net.

Polytypism and a conceptual model

Guggenheim *et al.* (1982) showed that two polytypes are present in both greenalite and caryopilite, the 1*T* and 1*M* polytypes. These polytypes were identified in the earlier work on the basis of powder X-ray diffraction patterns and are confirmed by the electron-diffraction patterns presented here. An earlier suggestion (Guggenheim *et al.* 1982) was that the presence of these two stacking sequences may relate in some manner to the structural modulation and are essential to the stability of the structural system. This suggestion is no longer plausible, because individual grains were found to be comprised of just one polytype.

Polytype identification by either powder X-ray or electron diffraction involves the use of $k = 3n$ reflections only, which reflect the occupancy pattern of the octahedrally coordinated cations. Thus, stacking sequences in greenalite and caryopilite are essentially defined by the relative positioning of adjacent octahedral sheets. Because the octahedral sheets include the coordinating anions (apical atoms of oxygen) that form a common junction with sheets of tetrahedra, it is possible to place constraints on the configuration of the tetrahedra.

Guggenheim *et al.* (1982) established, and this work supports, that these minerals have tetrahedra of a given layer having apical atoms of oxygen coordinating to one octahedral sheet and some to the other, *i.e.*, Si atoms occur in two adjacent sheets between adjacent octahedral sheets. For equal numbers of tetrahedra to coordinate to the two adjacent octahedral sheets, it is required that entire saucer-shaped islands of tetrahedra are inverted, rather than tetrahedra just at domain boundaries (Guggenheim *et al.* 1982). Therefore, inversions of tetrahedra constrain the positions of the apical oxygen in both adjacent octahedral sheets. The 1*T* and 1*M* polytypes as derived by Bailey (1969) have the proper configurations to allow both tetrahedral sheets to coordinate to adjacent octahedral sheets in greenalite

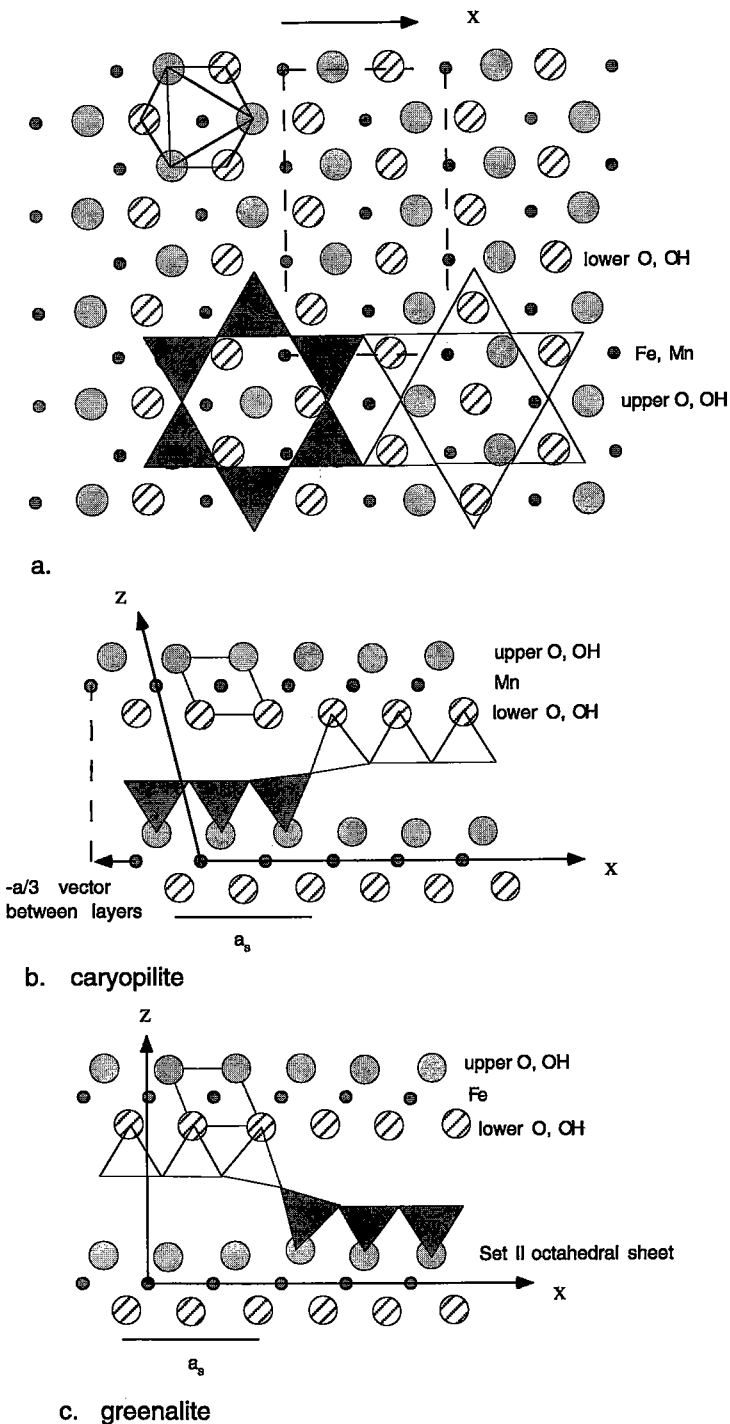


FIG. 6. a. Diagram of the greenalite-1*T* and the caryopilite-1*M* structures illustrating how the anions around the octahedra restrict possible positions of the silicate tetrahedra. The unit cell is of the subcell only. Diagrams in b) and c) are referred to a consistent "slant" to the octahedral sheet. See text for further discussion of the figure.

and caryopilite. We note that both configurations allow hydrogen bonds to form across the interlayer between hydroxyl ions of the octahedral sheet and basal atoms of oxygen of the tetrahedral sheet not coordinating to that octahedral sheet. Inversions of tetrahedra involving the three-fold ring in the model presented by Guggenheim *et al.* (1982, Fig. 8) cannot properly coordinate to adjacent octahedral sheets.

Figure 6 shows the two possible patterns (1*M* and 1*T*) of the oxygen atoms. All oxygen atoms are possible candidates to be apical oxygen atoms, regardless of the presence of (OH) in the ideal structure. Tetrahedron linkages along [100] are shown as four-membered rings, but the structure must have other linkage configurations also (see "Model structure" below); a series of four-fold connectors, or four-fold and eight-fold connectors, cannot establish a two-dimensional net with islands that are nearly equant in the layers parallel to (001). The 1*M* polytype drawing is based on a sheet of Mn-rich octahedra with $-a/3$ displacements, and the 1*T* is based on a sheet of Fe-rich octahedra.

Construction of a model structure

Guggenheim *et al.* introduced the ratio S/b , where S is half the superlattice b -dimension and b is the subcell b -parameter, comparable to the $9\text{-}\text{\AA}$ b -axis of normal layer silicates. The magnitudes of S and b vary inversely, with S decreasing as b increases. Larger values of S suggest larger islands of tetrahedra; thus,

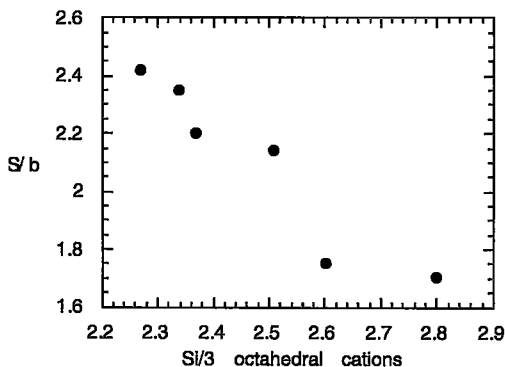


FIG. 7. Si content of greenalite - caryopilite versus S/b .

as S increases, the tetrahedral sheet has more extensive areas of "normal" 6-membered ring islands. The ratio of numbers of Si to octahedrally coordinated cations is 2:3 for a normal trioctahedral layer silicate. Modulations of the tetrahedral sheet occur where extra tetrahedra are inserted (to expand the sheet to "fit" to the octahedral sheet). The larger the discrepancy between the dimensions of the octahedral and tetrahedral sheets,

the greater the number of extra tetrahedra required: hence the Si:octahedra ratio increases. Figure 7 shows the ratio of silicon to octahedrally coordinated cation for six greenalite - caryopilite samples plotted against S/b . The well-defined inverse relation supports the hypothesis that as the octahedron edge increases in magnitude (b increasing), the supercell dimension (S) decreases because the islands of tetrahedra become smaller. Hence, more island inversions per unit area of the sheets are introduced, thereby resulting in more Si atoms per octahedrally coordinated cation. Thus, the islands are smaller and closer to one another in caryopilite than in greenalite.

To be consistent with S/b ratios and observed symmetry, the model presented here is based on a repeating element of a triangular island of rings of tetrahedra, as illustrated in Figure 8. As in normal phyllosilicates, each ring of tetrahedra is 6-fold. The size of each island and the distance between islands (which would be a lattice repeat if all such distances were the same) are presumed to be controlled by the mean octahedron size. Nearest-neighbor islands are typically inverted (Fig. 8). Possible positions for adjacent oppositely directed islands separated by four octahedra are shown in [001] projection in Figure 8. The open circles of Figure 8 represent octahedrally coordinated cations. An island of 13 tetrahedra (shaded hexagons representing the Si-Si linkages) coordinates to the octahedron's anions (not shown). Adjacent inverted islands (outline hexagons) coordinate to anions of the next layer. The long vectors span four octahedra, the three short vectors from the end of each long vector are directed to possible positions for the center of these three surrounding islands. The three islands pointed "up" have different relationships to the central island pointed "down" along each of its three sides. Possible connectors are 5-, 6-, 7-, and 8-member rings (Fig. 9).

The diffuse $k \neq 3n$ reflections, and the irrational spacing of the satellites with respect to the $k = 3n$ reflections, indicate that similar islands are positioned on centers randomly displaced from ideal positions (see discussion above on the Gaussian statistical distribution of domain centers). For greenalite, S ranges from 21 to 23 \AA as b ranges from 9.7 to 9.6 \AA . In the [010] direction, therefore, islands of the same orientation are spaced approximately every $3 \times 2S/b = 14.3$ octahedra (there are three octahedra per 9.6 \AA parallel to [010]). For caryopilite, the islands repeat every 10.4 octahedra ($6 \times 17/9.8$) to a first approximation. If all islands were equal in size, S/b would be 1.5 for three octahedra, 2 for four-octahedra vectors, and 2.5 for five octahedra. For greenalite, with $S/b = 2.38$, for example, a mixture of four- and five-octahedra vectors is proposed, whereas for caryopilite, with $S/b = 1.7$, a mixture of four- and three-octahedra vectors is suggested.

Figure 10 shows the upper and lower plane of anions of adjacent octahedral sheets and provides the

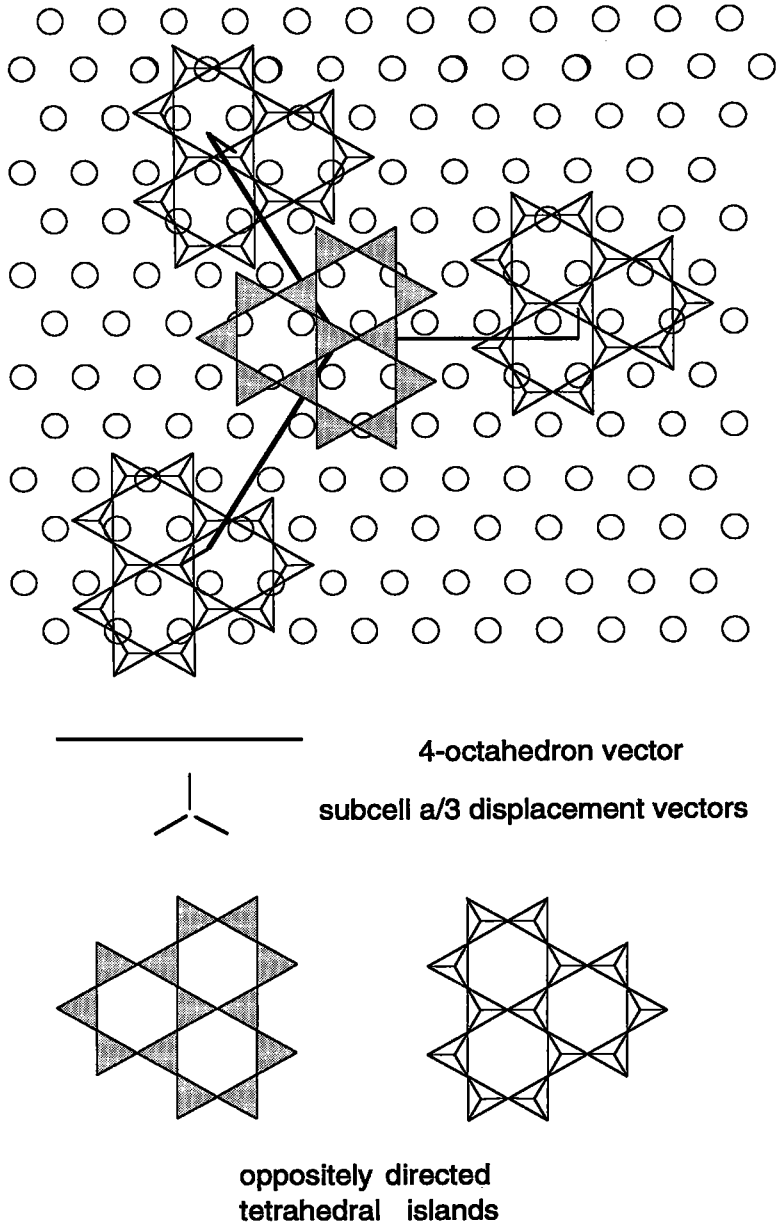


FIG. 8. Relative positions and linkages between islands of tetrahedra for greenalite – caryopilite (see text).

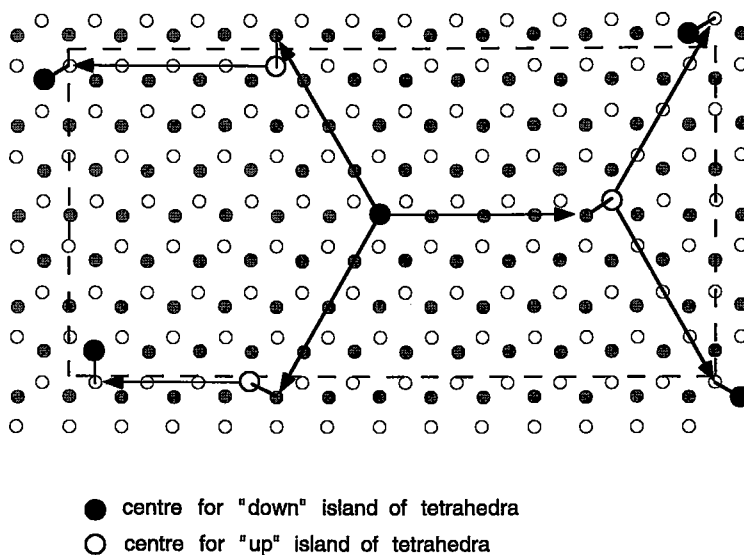


FIG. 9. Diagram illustrating possible linkages between oppositely directed islands of tetrahedra. The islands are positioned so octahedral sheets are in the greenalite relationship shown in Figure 6. Shaded circles represent Fe cations, stippled tetrahedra coordinate to anions above the cations but below the tetrahedral sheet, and outline tetrahedra coordinated to the underside of the octahedral sheet above. Arrows span four octahedra.

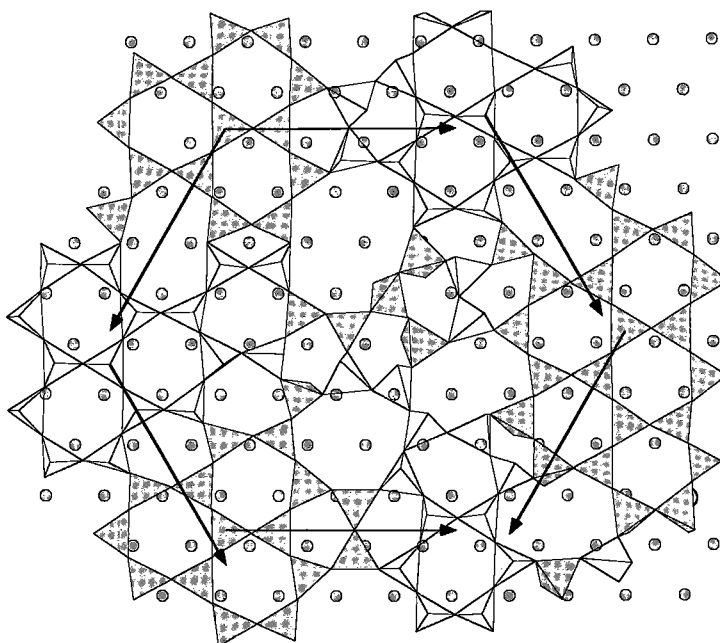


FIG. 10. Orthohexagonal average unit-cell, approximately 12.5 octahedra along [010]. Small circles are the positions of the octahedral anions on either side of the tetrahedral sheet. The long vectors span four octahedra (as in Fig. 8), or in one case, three octahedra. The short vectors are $a/3$ for the three equivalent hexagonal a -axes of the subcell. Random selection of the $a/3$ vectors places like island centers on an average "unit cell".

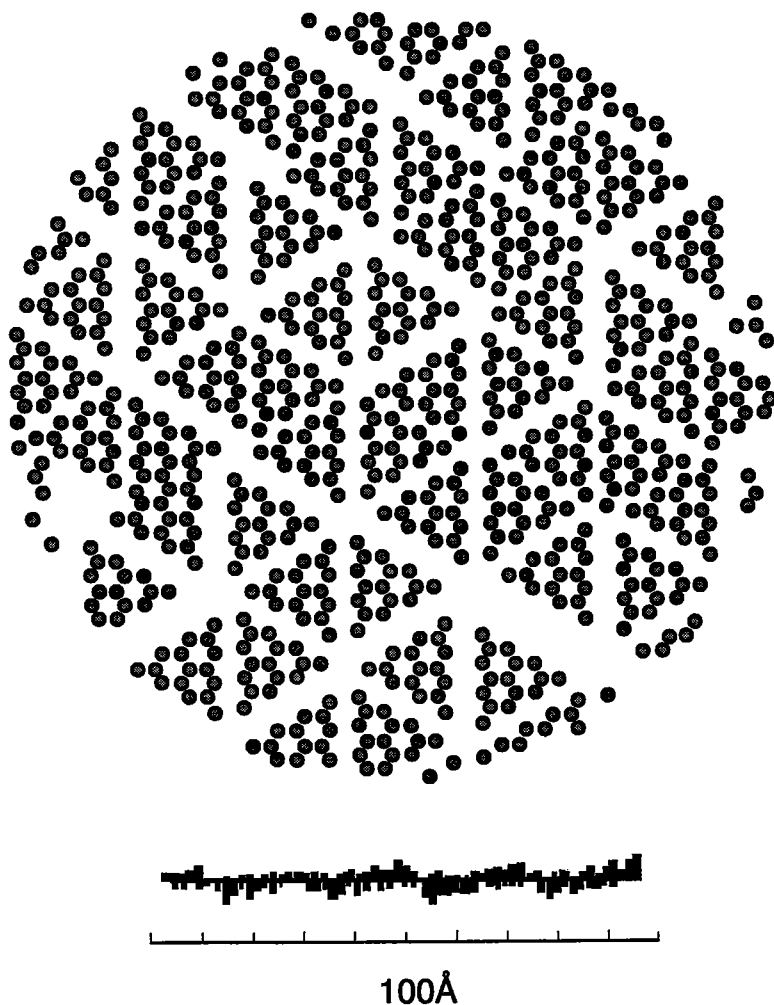


FIG. 11. Tetrahedron island model used to calculate the greenalite $hk0$ diffraction pattern. Tetrahedra connecting islands were not included. The histogram below shows the relative numbers of silicon atoms seen in projection along $[100]$, and may be compared to the changes in blackness seen between the octahedral sheets of the greenalite TEM image of Figure 5.

physical basis for the random positioning of island centers. The long vectors span four octahedra, as in Figure 8. The short vectors represent displacements from these vectors. Random positioning of island centers on one of the three anions at the ends of these vectors leads to an average "unit cell" (Fig. 10).

Figure 9 shows some possible linkages between islands, where islands are positioned as outlined above. Each group of linking tetrahedra has an analogue in other modulated layer silicates. Distorted 6-member rings with tetrahedra pointing in opposite directions are

known in ganophyllite, 4- and 8-member rings occur in serpentine (*e.g.*, antigorite), 4- and 12-member rings in pyrosmalite, and 5-member rings in bementite, minnesotaite, ganophyllite, and stilpnomelane.

An extended model was constructed to test these concepts against the electron-diffraction data. Two-dimensional (X - Y plane) computer models for caryopillite and greenalite (*e.g.*, Fig. 11) were developed. For caryopillite, the model was comprised of 3542 (Mn + Si) atoms only and was made for a crystal of 150 Å in diameter by positioning adjacent opposed islands at

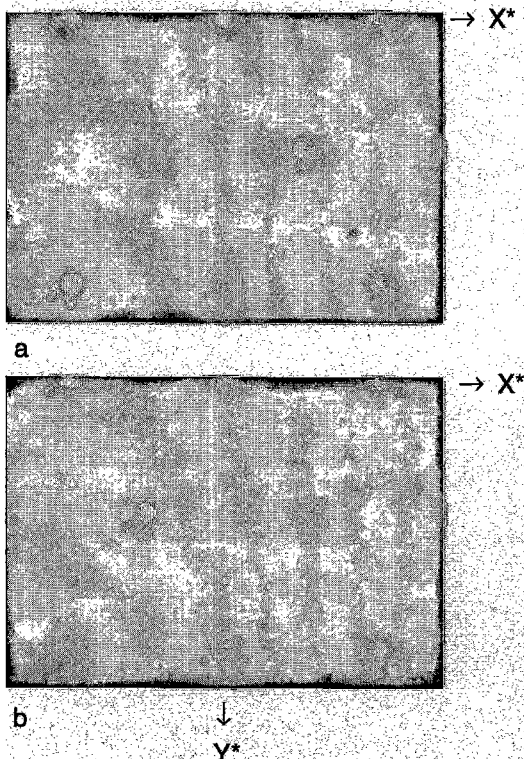


FIG. 12. Calculated Fourier transform of structure models for a) greenalite and b) caryopilite.

distances of three- or four-octahedron spacings to yield a mean separation of about 3.5 octahedra (caryopilite), which is equivalent to a S/b ratio of approximately 1.75. A similar model was made for greenalite, but with a mean separation of 4.5 octahedra (greenalite, $S/b = 2.25$). The model compositions are $Mn_{3,0}Si_{2,54}$, which may be compared to the Fallota caryopilite ($S/b = 1.75$) composition, $Mn_{3,0}Si_{2,6}$, and $Fe_{3,0}Si_{2,33}$, which may be compared to $Fe_{3,0}Si_{2,30}$ for Cartagena greenalite ($S/b = 2.3$).

The $hk0$ diffraction patterns (Fig. 12) were calculated by simple Fourier transform at intervals of $0.005 \sin\theta/\lambda$ using the 3542 atoms of the model. For example, in the one-dimensional Fourier term $\cos(2\pi hx)$, $h = ad^*$, thus $hx = axd^*$. The term ax gives the x -coordinate in \AA rather than the normal fractional value, $0 < x < 1$. Using this form for the Fourier summation, a model composed of any number of non-repeating atoms can be used to calculate diffraction intensities by finding the real-space coordinates of every atom relative to a selected origin [in this case, the model was built radially outward from (0,0)]. The reciprocal space variable d^* was then sampled at intervals of 0.005\AA^{-1} out to $d^* = 0.75 \text{\AA}^{-1}$ ($d = 1.33 \text{\AA}$), to build the continuous Fourier transform of the model. Constant scattering factors (= Z electrons for each

atom) for point atoms were used, and no corrections were made for temperature or geometric factors. Since Si positions are idealized, and the connecting Si atoms between islands and all the basal oxygen atoms are omitted, the resulting intensities are illustrated as a weighted reciprocal lattice. To more completely generalize the diffraction pattern, the calculated Fourier transform was superimposed on its (100) twin, which produced also a better match with Figure 12.

The three major features of the $hk0$ electron diffraction pattern are well simulated by the calculated pattern: the superlattice spacing ($S/b = 2.26$ for the greenalite transform, 1.79 for caryopilite), the intensity variations of the superlattice reflections, and the sectorial (three-part) appearance of the 02 reflection in caryopilite. Diffraction ripples caused by using a discrete-diameter model crystal were attenuated from the image by using a "Gaussian blur" with the computer application Adobe Photoshop.

Figure 13a shows a 30- \AA thick YZ projection of the model, and Figure 13c, its calculated diffraction pattern. This model used 21 layers in a crystal 160 \AA in diameter, composed of 14,500 atoms, including basal oxygen atoms. As with the $hk0$ simulation, no attempt was made to model the disordered region between islands of tetrahedra. The cations and anions of the octahedra repeat at regular intervals of subcell $b/6$ along [001]. Between the rows of octahedra, the silicon atoms and basal oxygen atoms are positioned with y -coordinates as in the model for Figure 11, and with z -coordinates in each island displaced from the ideal position to simulate doming of the tetrahedral sheet to allow for tetrahedron-octahedron misfit (Fig. 13b). From layer to layer, the tetrahedral sheet is displaced randomly by $-b_s/6$, 0, or $+b_s/6$, where s = subcell and the magnitude of $b_s/6$ is approximately equal to 1.6 \AA . This displacement ensures congruency between the sheets of tetrahedra and of octahedra. Evidence from the TEM images of "columns" of similar structure parallel to c^* suggests that the tetrahedra of successive layers have similar linkages; thus for the $0kl$ model, the same tetrahedral sheet was used for each layer, but with the $b/6$ random displacements. The resulting diffraction pattern shows two types of nodes as well as streaks. The stronger nodes (subcell nodes) are dominated by diffraction from the subcell of Fe, Mn cations, whereas satellites to the subcell reflections (superlattice nodes) are well defined and occur only near subcell nodes. The satellite reflections result from the dimensional difference between octahedral sheets and tetrahedra. Streaks at about $d^* = 1/5.2 \text{\AA}^{-1}$, $1/4.4 \text{\AA}^{-1}$, and $1/2.2 \text{\AA}^{-1}$ result from the random displacements of the tetrahedral sheets from layer to layer. The discontinuities in the streaks arise from the limited size of the model and from limiting displacements of tetrahedra to one of three possibilities. This pattern closely simulates the $0kl$ patterns for greenalite and caryopilite.

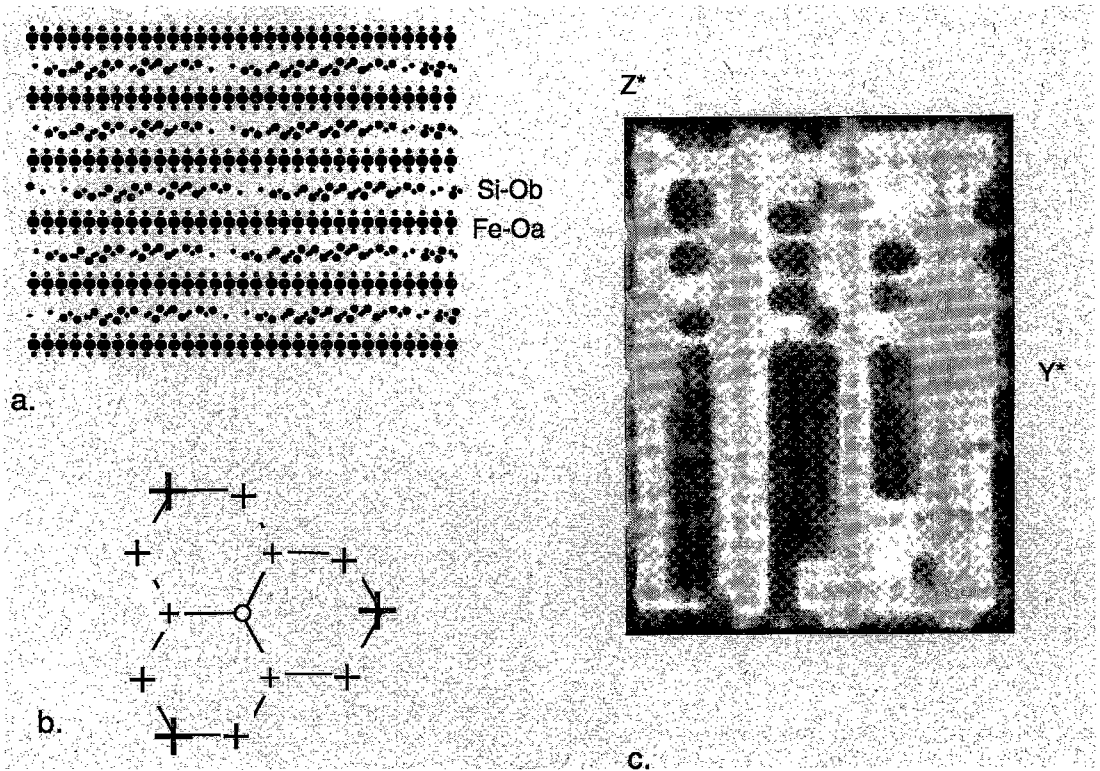


FIG. 13. a) Part of the model for the $0kl$ Fourier transform of greenalite, b) diagram of a tetrahedron island, + signs indicate the relative deviation of the silicon atoms from a flat plane; larger symbols have the greater difference from the center, and c) calculated $0kl$ diffraction pattern from a model 160 Å in diameter, 30 Å thick.

Thus it is shown that (a) the sharp superlattice nodes and (b) the marked decrease in intensity in higher-order superlattice nodes are a result of disorder in the spacings between domain centers, within small variations from the average.

CONCLUSIONS

Additional electron diffraction and image data have allowed more extensive development of a structural model for greenalite and caryopilite. The extreme positional disorder of tetrahedra is most apparent in high-resolution images. However, the stacking of the octahedra to form either the $1M$ or $1T$ polytypes indicates that there are constraints to the positioning of the domains of six-fold silicate rings. These constraints are defined by a series of displacement-vectors within (001). Within the constraints of possible displacement-vectors, the periodic placement of domains lacks order. Unfortunately, this prevents any precise description (*i.e.*, atomic coordinates) of the linkages of tetrahedra between domains; these areas are probably highly

disordered. Although linkages known from other modulated layer silicates were used to develop the model, there is no evidence that these actually exist in greenalite – caryopilite; any linkage between islands or no linkages at all yield similar simulated diffraction-patterns, as the island positions dictate the features of the diffraction pattern.

For equal numbers of tetrahedra to associate with adjacent octahedral sheets, entire islands are inverted rather than just domain boundaries, in contradiction to our earlier model (Guggenheim *et al.* 1982). However, much of that model remains valid, including saucer-shaped islands with regular doming of octahedra. Greenalite and caryopilite are similar to the serpentine-group minerals because they are trioctahedral phyllosilicates based on a 1:1 layer (7 Å). In addition, at least limited portions of the structure (*i.e.*, the islands) have 6-fold rings of tetrahedra, which in part control the stacking of adjacent octahedral sheets to produce polytypes consistent with the platy serpentines. In contrast to the serpentines, however, greenalite and caryopilite have dome-like islands and

short-range and long-range disorder caused by domain-boundary linkages and domain positioning. Domain boundaries, which make up large portions of the structure, are clearly not based on 6-member ring arrangements of tetrahedra. These structural modulations lead to chemical formulae that deviate considerably from the stoichiometry of serpentine minerals. Although greenalite and caryopilite are clearly modulated phyllosilicates, we leave open the question of categorizing these minerals as serpentines.

ACKNOWLEDGEMENTS

This study was supported by the Petrology and Geochemistry Program and the U.S. – Australia Co-operative Science Program of the National Science Foundation under grant #EAR-9003688. We thank the University of Illinois Research Resources Center for the use of the JEOL 100CX microscope and the Research School of Chemistry (ANU) for the use of the JEOL 200CX microscope. We thank also M.G. Rasmussen, University of Washington, and R. Skirrow, Australian National University, for providing us with samples and electron-microprobe data. We acknowledge the late S.W. Bailey, University of Wisconsin – Madison for reviewing an early version of the manuscript. We thank D.R. Peacor, University of Michigan, and P. Leavens, University of Delaware, for reviewing the final version.

REFERENCES

BAILEY, S.W. (1969): Polytypism of trioctahedral 1:1 layer silicates. *Clays Clay Minerals* **17**, 355-371.

FRONDEL, C. (1955): Two-chlorites: gonyerite and melanolite. *Am. Mineral.* **40**, 1090-1094.

GUGGENHEIM, S. & BAILEY, S.W. (1989): An occurrence of a modulated serpentine related to the greenalite-caryopilite series. *Am. Mineral.* **74**, 637-641.

_____, _____, EGGLETON, R.A. & WILKES, P. (1982): Structural aspects of greenalite and related minerals. *Can. Mineral.* **20**, 1-18.

_____, & EGGLETON, R.A. (1987): Modulated 2:1 layer silicates: review, systematics, and predictions. *Am. Mineral.* **72**, 724-738.

_____, & _____ (1988): Crystal chemistry, classification, and identification of modulated layer silicates. In *Hydrous Phyllosilicates Exclusive of the Micas* (S.W. Bailey, ed.). *Rev. Mineral.* **19**, 675-725.

GUINIER, A. (1963): *X-Ray Diffraction in Crystals, Imperfect Crystals, and Amorphous Bodies*. W.H. Freeman and Company, San Francisco, California.

RASMUSSEN, M.G., EVANS, B.W. & KUEHNER, S.M. (1998): Low-temperature fayalite, greenalite, and minnesotaite from the Overlook gold deposit, Washington: phase relations in the system FeO-SiO₂-H₂O. *Can. Mineral.* **36**, 147-162.

WARE, N. (1991): Combined energy dispersive and wavelength dispersive quantitative electron microprobe analysis. *X-ray Spectrometry* **20**, 73-79.

Received November 27, 1996, revised manuscript accepted May 23, 1997.